RESEARCH ARTICLE | JUNE 16 2023

Advancing the mechanical integrity and fragmentation behavior of reactive projectiles

Alan Williams ; Mackenzie Geigle ; Timothy Fah ; Surojit Gupta ; Michelle Pantoya

Journal of Applied Physics 133, 235901 (2023)
https://doi.org/10.1063/5.0155206

Journal of Applied Physics ARTICLE pubs.aip.org/aip/jap

Advancing the mechanical integrity and fragmentation behavior of reactive projectiles

Cite as: J. Appl. Phys. 133, 235901 (2023); doi: 10.1063/5.0155206
Submitted: 18 April 2023 · Accepted: 4 June 2023 ·
Published Online: 16 June 2023

View Online Export Citation CrossMark

Alan Williams,[1] Mackenzie Geigle,[2] Timothy Fah,[2] Surojit Gupta,[2] and Michelle Pantoya[1,a)]

AFFILIATIONS

[1]Department of Mechanical Engineering, Texas Tech University, Lubbock, Texas 79407, USA
[2]Department of Mechanical Engineering, University of North Dakota, Grand Forks, North Dakota 58202, USA

[a)]**Author to whom correspondence should be addressed:** Michelle.pantoya@ttu.edu

ABSTRACT

A multivariant statistical approach was used to identify treatment conditions that improve the survivability of structural reactive material (SRM) projectiles upon launch and enhance energy release upon impact. The study included both mechanical testing of projectiles as well as their reactive characterization. The projectiles were launched in a high-velocity impact-ignition testing system and impacted an anvil for vented chamber calorimetry. This study examined a link between ultimate compressive stress and combustion performance. Two treatments were applied to consolidated aluminum projectiles including annealing and addition of silica (SiO_2) inclusions. Results showed annealing at moderate temperatures resulted in intact SRM projectiles upon launch. Adding small concentrations (1–2 wt. %) of SiO_2 to the SRM promoted fragmentation and combustion performance upon impact. Compared to the untreated projectiles, annealing with SiO_2 inclusion processing treatments improved the energy conversion efficiency from 37–84% (for untreated projectiles) up to 54–98%. Increasing interparticle dislocation recovery by annealing while balancing inclusions promoting fragmentation upon impact was the key to optimizing combustion performance for SRM ballistic impact applications.

INTRODUCTION

Structural reactive material (SRM) projectiles are formed from consolidating powder metal fuels and commonly include aluminum. Upon high velocity impact, the projectile fragments and oxidizes to generate chemical as well as kinetic energy. Fragmentation is critical for combustion, and a smaller size distribution of reactive fragments correlates with greater combustibility.[1] Also, a projectile's fracture and fragmentation behavior are a function of material strength, often characterized by ultimate compressive stress (UCS).[2,3] The energy released upon impact, fragmentation, and reaction can be harnessed for a variety of applications, such as neutralizing threats for military defense.[4,5] SRM projectiles can also be designed to disperse upon impact and act as a biological agent combatant or obscurant.[6,7]

Projectiles are frequently tested in high-velocity impact ballistic systems, where a projectile can be launched into an instrumented chamber at velocities up to 2000 m/s.[3,8,9] A recurring challenge in ballistic testing is partial fracture or disintegration of the projectile before reaching or penetrating the target.[8,10] Many researchers address material integrity issues by including polymer additives, such as polytetrafluoroethylene (PTFE), at weight percentages exceeding the fuel concentration.[10,11] The polymer acts as a binder and maintains the structure of the particulate matrix even under extreme loading conditions associated with projectile launch. For example, using QuickLOAD muzzle velocity prediction software,[12] the projectile experiences approximately 275 kPa maximum pressure generated by the shotshell powder under the experimental conditions. When high-energy and high-density are required, inclusion of a binder limits the fuel available for reaction and reduces the density and kinetic energy of the projectile. Metallurgical processing treatments such as annealing offer an alternative to binder addition for improving projectile survivability upon launch.[3]

In a ballistic environment, a projectile experiences significant confining pressures, along with axial compression from propellant pressurization. Wiegand *et al.*[13] investigated varying the confining pressurization experienced by an energetic projectile to understand its mechanical response, such as cracking, fracturing, and yielding. They discovered that as the confining pressure increased, the stress required at any strain to cause crack damage increased accordingly. In other words, confining pressure inherent in the barrel of ballistic applications is effective at inhibiting fracturing of a projectile. Based on Wiegand *et al.*,[13] small improvements in mechanical properties of the projectile may inhibit cracking and enable the projectile to remain intact after launch.

The objective of this study is to identify multivariant pellet processing treatments that will produce consistent and improved combustion performance compared to untreated (baseline) pellets. Specifically, two factors are considered: annealing the consolidated powder projectiles and adding silica (SiO_2) particles at varied concentrations. Annealing is intended to increase the ultimate compressive stress enough (i.e., >5%–10% relative to untreated projectiles) for the pellet to remain intact upon launch. Silica inclusions are intended to provide dislocations within the matrix to induce fragmentation upon impact.

From a reactivity perspective, any gain in energy conversion is noteworthy, but linking the gain in reactivity to a mechanism for producing the gain is most important. The proposed mechanism hypothesized here is that any single projectile treatment that results in reduced fracture after launch would accompany reduced fragmentation after target impact, thereby limiting the overall energy released. Therefore, the approach applied here combines variants such as projectile annealing treatment to bolster ultimate compressive stress via interparticle dislocation recovery, and additives to stimulate fragmentation and combustion after impact. Because multiple factors influence the coupled outcomes, a statistical design of experiments (DOEs) approach was used for regression analysis of projectile performance.[14]

VARIANTS

Annealing

To promote intact projectiles after launch, the consolidated powders were annealed. Kline and Hooper showed that annealing consolidated aluminum powder projectiles at 200 °C increased the tensile strength and fracture toughness, while significantly reducing finer fragmentation when launched into thick steel targets.[3] The increased strength observed by Kline and Hooper[3] was attributed to dislocation recovery in the aluminum particle matrix and no sintering was observed at 200 °C. The effects of annealing consolidated powders are generally attributed to crack healing, residual stress healing, and dislocation recovery.[15–19]

Additives

Another variant to promote fragmentation and energy release upon impact is the inclusion of interstitial, hard particles added to the aluminum particle matrix.[20] Aluminum is a soft metal while ceramics, such as silica are hard. The interface of hard and soft materials presents a discontinuity for manifesting stress when energy is applied to the bulk composite. Stress concentrators such as silica additives are potential sites for fatigue crack nucleation.[21,22] Chen and Tokaji found that depending on the size and morphology of an additive particle, cracks will initiate along interfaces between the additive and metal matrix because discontinuities between material properties promote fracture.[23,24] While loading dynamics are more extreme in a ballistic environment compared to fatigue loading in a bulk composite, similar fracture mechanics principles apply.

TABLE I. Design of experiment (DOE) treatment factors and levels.

Factor	Treatment	Units	Levels	Level 1	Level 2	Level 3
A	Annealing	°C	3	350	450	550
B	SiO_2 additive	wt. %	3	0	1	2

EXPERIMENTAL

Design of experiments approach

To accomplish the objective of pellet survivability after launch while promoting fragmentation and energy release upon impact, two factors were considered in the design of experiments (DOEs): annealing condition and additive concentration. The two factors and their respective design levels are shown in Table I.

Given the finding that annealing at 200 °C resulted in improved mechanical properties,[3] three levels of annealing temperatures were considered: 350, 450, and 550 °C. It is noted that the aluminum melting temperature is 660 °C such that all levels were selected to induce residual stress healing and dislocation recovery within the matrix. Annealing was performed in a tube furnace (MTI Corp., model OFT-1200X) that was vacuum pumped and filled with argon (three cycles). Each pellet was annealed to the specified temperature at 10 °C/min, held for 30 min, and then air-cooled in an ambient environment.

The three levels of additive concentration ranged from 0–2 wt. %, as indicated in Table I. The additive concentration should ideally be as low as possible to induce fragmentation upon impact and negligibly contribute to the overall mass of the projectile. In this case, silica was selected as the additive based on its hardness relative to aluminum (i.e., Mohs' hardness 7 compared to 2.75, respectively.[21] The hypothesis is that the interface discontinuity in hardness will incite fragmentation that will enhance reactivity upon impact.

A response surface methodology (RSM) informed the experimental test matrix. In statistics, an RSM allows analysis of the relationship between multiple explanatory variables (i.e., factors in Table I), and one or more response variables (i.e., ultimate compressive stress and energy). This approach is particularly useful to inform a sequence of experiments to obtain information about the trends in optimized response variable behavior. It is noted that a similar DOE approach using a RSM was applied in a numerical investigation of a multi-layered plate under ballistic impact.[25] Park *et al.*[25] used an equivalent plastic strain response variable for optimization of the plate variables resisting penetration. Here the RSM informs the test matrix thereby reducing the number of potential experiments required to evaluate trends toward optimized performance. When the number of tests in an experimental test matrix must be limited by practicality, randomization of replicates is a common technique to prevent systematic biases between experimental groups and motivation for using the DOE software for this analysis.

TABLE II. Design of experiments treatment test matrix.

Test	Annealing (°C)	SiO_2 (wt. %)	Test	Annealing (°C)	SiO_2 (wt. %)
1	350	0	8	450	2
2	350	0	9	450	2
3	350	1	10	550	0
4	350	2	11	550	0
5	450	0	12	550	1
6	450	1	13	550	1
7	450	1	14	550	2

The test matrix is presented in Table II and derived from the factors and levels indicated in Table I. In addition to the tests in Table II, baseline testing for 100% Al consolidated pellets (i.e., without additives or annealing) were also performed for reference.

Ballistic impact testing

Spherical aluminum (Al) powder with a nominal particle diameter of 3.5 μm was supplied from Valimet Inc., Stockton, CA, USA (Product No. H2, Batch No. 19-006). The silicon dioxide SiO_2 powder was nominally 3.5 μm particle size and supplied from Alpha Aesar (Lot No. K07N37, CAS No. 7631-86-9).

The Al and SiO_2 powders were combined and placed into a speed mixer (FlackTek Inc., DAC 150.1 FVZ-K) operated at 1000 revolutions per minute for 2 min. The recovered mixture or pure Al powder (e.g., both 1.7 g) was loaded into a 10 mm pellet press die set and placed in a Carver Auto Series automated hydraulic press. The press applied 20 kN into the die set, dwelled for 60 s, and produced a pellet 1 cm diameter by 1 cm length. The final projectile achieved 82% theoretical maximum density. Representative images of the pellets are shown in Figs. 1(a)–1(c). Each pellet was wrapped in a nylon sabot and loaded into a.410 shotshell, illustrated in Fig. 1(d).

Each shotshell (Fig. 1) was loaded with 2.2 g of propellant powder for a projectile velocity of 1.25 km/s. Projectiles were launched using a high-velocity impact-ignition test system (HITS). Photographs of HITS are shown in Fig. 2.

After the projectile leaves the barrel, it passes through thin aluminum foil break screens that trigger the high-speed camera and lighting system, shown in Fig. 2(a). The projectile then passes into a rectangular visual catch chamber [Fig. 2(b)] that contains a steel divider plate to create a confined volume. The divider plate has a 3.6 cm diameter hole in the center allowing the projectile to pass into the confined region. After passing through the divider plate, the projectile travels through the chamber and impacts a hardened steel anvil [Fig. 2(b)]. Quasi-static pressure is measured in the confined region along with visual observation of the impact event.

Diagnostics for this experiment include two dynamic pressure sensors (PCB model 113B26) positioned on top of the chamber and record data at 110 kHz. A duplicate sensor system provides repeatability if one sensor were to fail or show an anomaly post-processing. In this experiment, one sensor performed as expected and was used for all pressure calculations while the second sensor confirmed data acquisition.

A Phantom v2512 high-speed monochrome camera recorded the impact event. The camera recorded at 512 × 768-pixel resolution, 50 000 frames per second, with 1 μs exposure. The camera was aligned perpendicular to the direction of the projectile path and captured the entire combustion region of the visual chamber, past the divider plate, as well as a small region before the divider plate. The camera position allowed observation of any reaction that may occur due to premature fragmentation. To improve visibility and video data, a diffusion screen was placed on the far outer side of the visual chamber, relative to the camera. The window of the chamber was 1 cm thick polycarbonate to prevent blowout and mated to a 3 mm sheet of polycarbonate for cost-effective replacement after each shot.

Data analysis

In ballistic impact experiments, energy released is determined by a technique called vented chamber calorimetry, discussed in detail by Ames *et al.*[26] The main pressure metric used to calculate

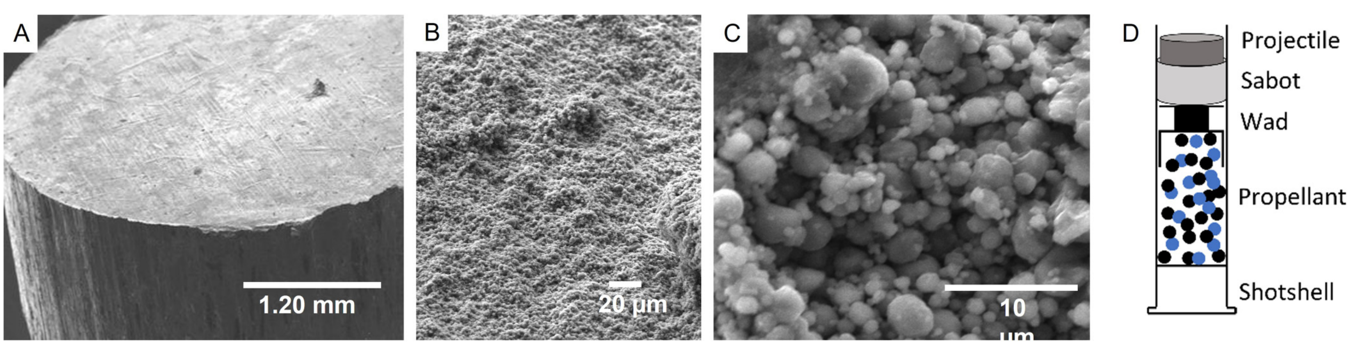

FIG. 1. (a) Light microscope image of pellet. (b) SEM image of Al + 2 wt. % SiO_2 annealed to 450 °C. (c) Higher resolution SEM image of Al + 2 wt. % SiO_2 pellet annealed to 450 °C. No sintering is observed. SiO_2 particles do not appear distinct from Al particles at the surface. (d) Schematic of assembled shotshell, including pellet projectile, sabot, wad, and propellant.

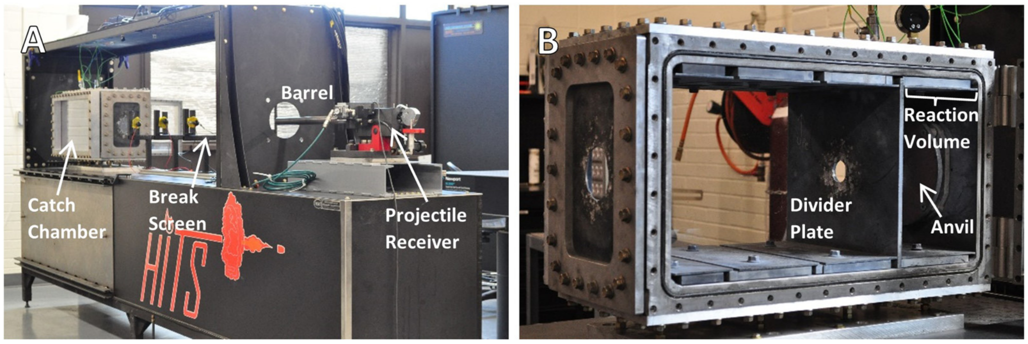

FIG. 2. (a) Fully assembled high-velocity impact test system and (b) closeup image of catch chamber for combustion visualization and measurements.

the energy release is peak pressure, i.e., the highest pressure measured.

The Ames[26] vented chamber calorimetry energy deposition method assumes quasi-static peak pressure (P) is related to maximum gas temperature (T_{gas}) from the ideal gas equation of state [Eq. (1)]

$$T_{gas} = \frac{PV_m}{R}. \tag{1}$$

In Eq. (1), R is the universal gas constant and V_m is the molar volume of gas. For all experimental pressure data, the chamber volume is 13.22 l and the projectile mass is 1.738 g. The molar volume includes consideration of the air in the chamber and the vapor phase products formed in the aluminum oxidation reaction [Eq. (2)]

$$\mathrm{Al} + \frac{3}{4}\mathrm{O_2} \rightarrow \frac{1}{2}\mathrm{Al_2O_3} + 838.35\,\mathrm{kJ/mol}. \tag{2}$$

It is noted that the 1–2 wt. % SiO_2 additive can react with Al at elevated temperatures with a heat of combustion that is small relative to O_2 (i.e., 58 compared with 838/35 kJ/mol, respectively). In this analysis, only O_2 oxidation is considered an upper maximum of chemical energy potentially available. The gas phase energy (E_{gas}) is calculated from the temperature difference (assuming the initial ambient temperature to be 298 K) and the heat capacity, estimated as (5/2)R, as shown in Eq. (3),

$$E_{gas} = \frac{5}{2}R(T_{gas} - 298\,\mathrm{K}). \tag{3}$$

Estimating condensed phase energy (E_{cond}) is an extension of the gas phase energy analysis presented by Ames.[26] Two limiting cases are considered for the condensed phase energy calculations. In both limiting cases, Eq. (4) is applied, and the heat capacity (C_p) is approximated for alumina at an average elevated temperature of 2000 K.[27] The lower limit assumes the temperature of the condensed phase products (T_{cond}) is equivalent to the air temperature (using the molar volume of air only) evaluated from peak pressure measurements [Eq. (1)]. The upper limit assumes the condensed phase products correspond to the boiling temperature of alumina (i.e., 3250 K)

$$E_{cond} = C_P(T_{cond} - 298\mathrm{K}). \tag{4}$$

The total energy deposited is the sum of the condensed and gas phase energies. The calculation is presented as a range spanning the lower and upper limits for the condensed phase energy calculation.

The energy conversion efficiency is the total energy deposited divided by the potential chemical energy, which is 838.35 kJ/mol corresponding to complete aluminum oxidation shown in Rn. (1). Energy conversion efficiency is also reported for the range of limiting cases of condensed phase energy.

The kinetic energy (KE) of impact is additionally calculated for the impact velocity (V = 1250 m/s) and projectile mass (m = 1.738 g) from Eq. (5),

$$KE = \frac{1}{2}\,\mathrm{mV}^2. \tag{5}$$

The projectile KE is 780 J/g or 21 093 J/mol of aluminum, and a fraction of the chemical energy potentially available [i.e., 838 350 J/mol, see Eq. (2)]. The above analysis is focused on the chemical energy released and does not include KE. However, including KE increases the total energy deposited such that the energy conversion efficiency is roughly increased by 1%–2%.

Mechanical testing

Mechanical compression tests were performed in a Shimadzu AG-IS UTM (Shimadzu AG-IS UTM, Shimadzu Scientific Instruments Inc., Columbia, MD). Pellets were examined in triplicate for standard deviation in the average measurement. Each pellet was tested using a 50 kN load cell at a deflection rate of 5 mm/min and stress was plotted as a function of displacement. Ultimate compressive stress (UCS) is defined here as the maximum stress at which a sample fails.

SEM analysis

A Zeiss Crossbeam 540 Scanning Electron Microscope (SEM) was used for microstructure analysis. Four samples were examined: untreated Al and three samples each containing 2 wt. % SiO_2 with annealing treatments of 350, 450, and 550 °C, respectively. The consolidated projectiles were examined by crushing the pellets using a manual arbor press. While the rate of impact is orders of magnitude less than the extreme load of ballistic impact, the results provide insight into potential debonding mechanisms associated with SiO_2 interfaces.

RESULTS

Pellet survivability

The qualitative survivability outcome of treatments is presented in Fig. 3. The first three images [Figs. 3(a)–3(c)] show the pre-impact fracturing of untreated, baseline aluminum pellets as they travel through the chamber. Each baseline pellet passes through a hole in the divider plate and a significant "pre-reaction" occurs on the face of the plate. The pre-reaction is seen by the bright flames outside of the chamber resulting from fragment ignition upon impact. The degree of pre-reaction varies and is a function of pellet disintegration before reaching the target. While the likelihood of pre-reaction outside the chamber is high for untreated pellets, annealed pellets survived launch intact with no observable pre-reaction.

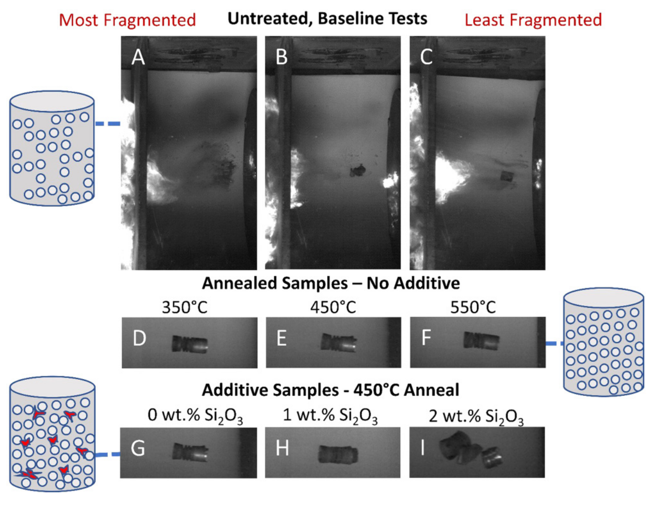

FIG. 3. Pellet survivability across treatments. (a)–(c) Images from untreated projectiles showing a range of fracturing from nearly complete disintegration (most fragmented) to partial fragmentation (least fragmented). All forms of early fracturing result in pre-reaction before impact seen from bright flames in each image. (d)–(f) Images from the annealing treatments of 350, 450, 550 °C, respectively, with no SiO_2 additive. (g)–(i) Represent SiO_2 additive treatments with levels of 0, 1, 2 wt. % and annealing at constant 450 °C. Cartoons illustrate potential alignment of particles within the pellets that result from treatments. Red particles represent SiO_2, and white circles represent aluminum.

The next three images in Figs. 3(d)–3(f) show the effect of annealing (350, 450, 550 °C, respectively) on pellet survivability and without SiO_2 additive. The final three images in Figs. 3(g)–3(i) show the effect of SiO_2 additive on survivability, when the annealing temperature is held constant at 450 °C. All treatments illustrated in Figs. 3(d)–3(i) show the pellet survives launch intact [e.g., produces no evidence of pre-reaction as shown in Figs. 3(a)–3(c)].

To compare pressure characteristics of treated to baseline pellets, the pressure response for five baseline aluminum pellets is shown in Fig. 4. Pressure response is widely variable, largely due to disintegration of the pellet upon launch and probability that aluminum reaches the chamber and reacts. The wide variability shown in Fig. 4 is compelling evidence for the need to design treatments that improve processing projectiles that produce consistent and reliable responses in ballistic applications.

From Fig. 4, the probability that the pellet will remain intact throughout launch (survive) and reach the target is 1:5. The one surviving pellet is shown visually in Fig. 3(c) and in curve 2 of Fig. 4. Interestingly, this surviving pellet has one of the lowest peak pressure measurements. Higher peak pressure baseline pellets result from more intense Al fragmentation post-launch and post-impact. In Fig. 4, the intact pellet (labeled 2) did not fragment in a way to optimize chemical energy released and produced a low peak pressure. The variability in pressure response in Fig. 4 is directly related to the mechanical integrity (survivability) of the pellet upon launch and fragmentation upon impact. From the data in Fig. 4, the average peak pressure for baseline pellets is 48.30 kPa.

Pressure response

As seen in Fig. 5(a), the DOE statistical analysis results in a contour map describing the multivariant effect of annealing temperature and SiO_2 concentration on peak pressure. Each data point corresponds to a specific treatment. The colorized oval rings represent increasingly higher peak pressure as they converge. Blue regions indicate more limited combustibility (lower peak pressure),

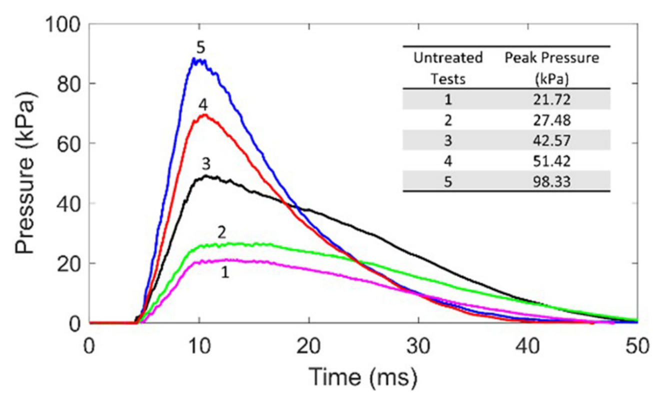

FIG. 4. Pressure as a function of time for untreated, baseline projectiles. Five tests show data vary widely for pressure response in replicate tests. The inset shows corresponding peak pressure measurements. Results indicate a need for pellet processing treatments to produce repeatable, reliable performance.

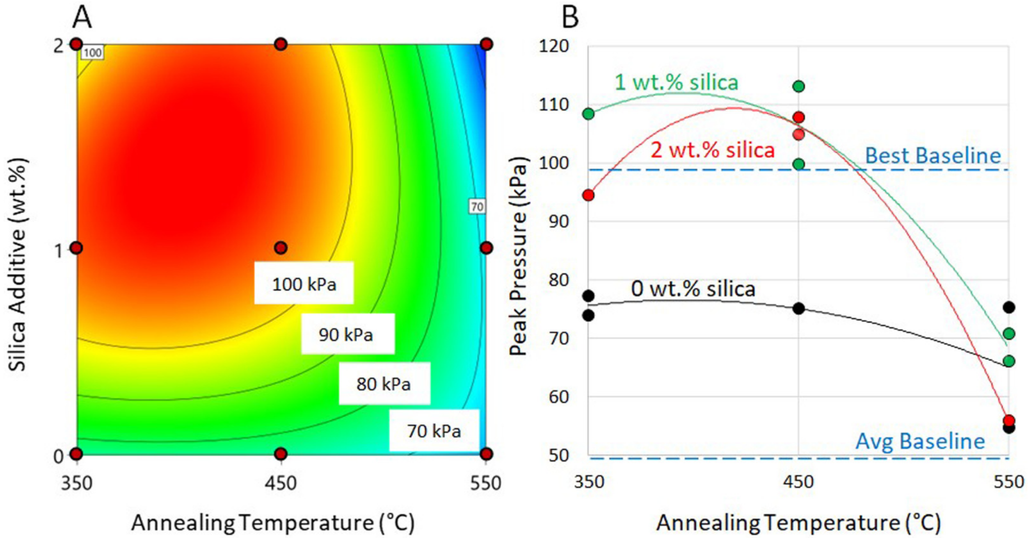

FIG. 5. (a) Contour plot showing the effect of projectile treatments: annealing temperature and SiO_2 wt. % on peak pressure using a cubic fit. Pressure contours are labeled. (b) Interaction plot between annealing temperature and SiO_2 concentration, and the effect on peak pressure response using a 2nd order polynomial fit. Dashed lines represent the best baseline and average baseline cases.

and the orange/red regions represent increased combustibility (higher peak pressure). The same data are represented by their pressure traces, and the same trends are observed in Fig. 6.

For reference (Fig. 4), the highest performing baseline projectile produced 98.33 kPa peak pressure [dashed line in Fig. 5(b)] but the average, 48.03 kPa, is below the minimum in Fig. 5(b), i.e., 50 kPa. In Fig. 5(b), in the case for annealing temperature progressively increased from 350 to 550 °C with no SiO_2 (0 wt. %), the peak pressure consistently underperforms compared to the best baseline pellet, producing peak pressures below 80 kPa. While annealing improves survivability upon launch, pellet fragmentation upon impact is more limited resulting in less reactive projectiles and lower peak pressure.

At the maximum annealing temperature treatment (550 °C) with SiO_2 varied from 0 to 2 wt. %, the projectiles also underperform relative to the best baseline case (i.e., <80 kPa). The 550 °C treatment may need a higher concentration of inclusions to produce the fragmentation upon impact needed to elevate peak pressure after impact.

When a 350–450 °C annealing treatment is applied and SiO_2 is added (1–2 wt. %), the peak pressure exceeds the best baseline case. Annealing the projectiles between 350 and 450 °C for 30 min while including 1–2 wt. % SiO_2 produced ideal conditions for SRM projectiles to survive launch while enhancing fragmentation and reactivity upon impact, in comparison to the improbable but most successful baseline projectile.

Energy conversion

Energy metrics are shown in Table III based on calculations described in Eqs. (1)–(4). To compare treatments, four categories of samples were analyzed: average results from (1) baseline, (2) annealed, (3) 1 wt. %, and (4) 2 wt. % SiO_2 additive projectiles. Since all annealed projectiles consisting of 0 wt. % SiO_2 produced similar peak pressure, the annealed group is the average of annealed data with 0% SiO_2 across all temperatures. The 1 wt.% SiO_2 data performed similarly at 350 and 450 °C annealing temperatures, so the 1 wt. % SiO_2 group is the average over these annealing temperatures. Similarly, the 2 wt. % SiO_2 group is the average over 350 and 450 °C annealing temperatures.

Table III shows adding SiO_2 and annealing improves energy conversion efficiency. The energy conversion efficiencies reported in Table III for the lower limit correspond well with previous reports for thermite and intermetallic pellets assuming similar conditions (i.e., product temperature is equivalent to gas temperature).[28] As noted in Croessmann *et al.*,[28] the lower limit is an underestimate because energy transferred from reacting materials to the gas requires the condensed product temperature to be higher than the gas.

Mechanical testing

Mechanical stress curves for the baseline, annealed, and annealed with SiO_2 projectiles are shown in Fig. 7. Ultimate compressive stress (UCS) is calculated at the peak stress value. At 350 °C, the projectile is more ductile with a slightly higher average UCS compared to the baseline [Fig. 7(a)]. As annealing temperature increases, the ductility and UCS also increase relative to the baseline [Figs. 7(b) and 7(c)]. For higher annealed samples, the stress curve does not peak, thus UCS is the highest value recorded on the curve.

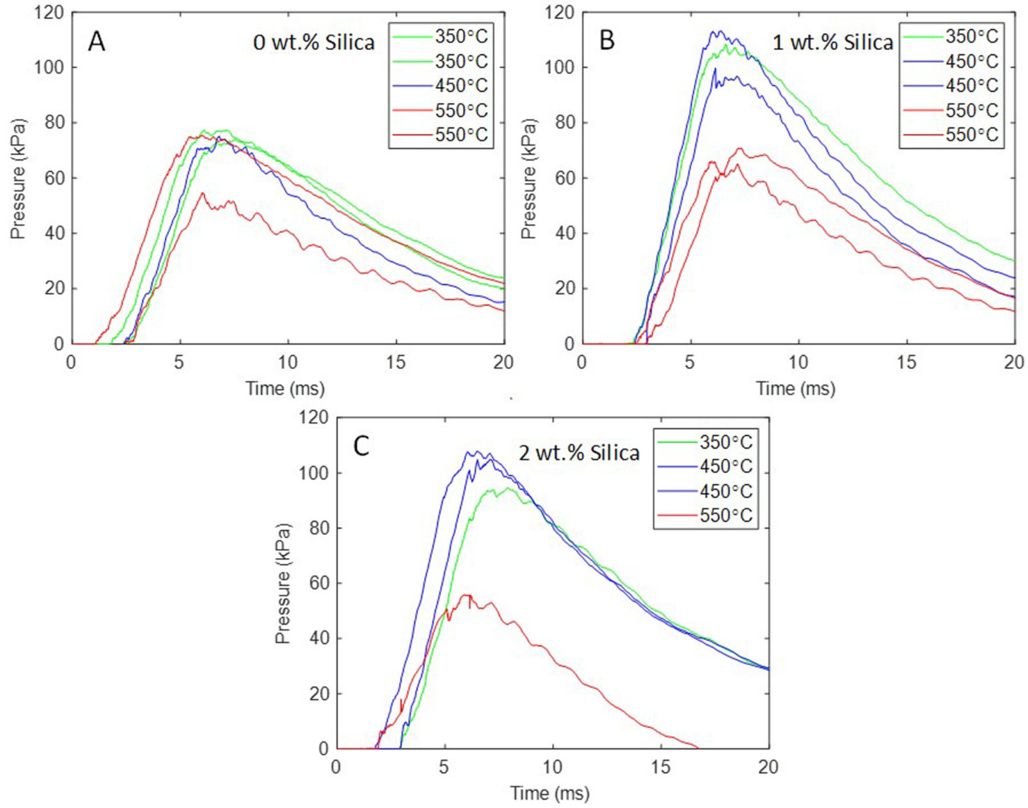

FIG. 6. All pressure data for treated projectiles as indicated: green curves correspond to 350 °C annealing, blue is 450 °C annealing, and red is 550 °C annealing. Plot (a) includes data for 0, (b) 1, and (c) 2 wt. % SiO_2.

Adding SiO_2 reduces ductility and UCS for all annealing treatments, as shown in Fig. 7(d). The reduction in UCS with additive is consistent with more fragmentation upon impact leading to higher peak pressure. While the average UCS for the baseline projectile is within the range of all treatments, the stochastic behavior of baseline projectiles is not desirable.

Figure 7(d) shows that UCS alone is not an indicator of optimal projectile performance. The most successful projectiles (350 and 450 °C annealing with 1 wt. % SiO_2) have the same UCS as the baseline. However, the annealing treatment significantly increased the UCS relative to the baseline, indicating improved strength and survivability of the annealed projectile upon launch. The role of the SiO_2 additive is to intentionally embrittle the projectile upon impact. The trend of reduced UCS with SiO_2 upon annealing is consistent with the energy conversion efficiency in Table III. Figure 7(d) and Table III indicate the coupled effects of annealing and inclusions on mechanical properties leading to improved projectile performance.

TABLE III. Measured pressure and calculated energy for treated projectiles compared to baseline. Note maximum chemical potential energy theoretically possible is 838.35 kJ/mol. Ranges are calculated for lower and upper limiting cases of condensed phase temperature corresponding to air temperature for peak pressure measurements and alumina boiling temperature, respectively.

Sample group	Absolute peak pressure (kPa)	Gas energy (kJ/mol)	Condensed energy (kJ/mol)	Total deposited energy (kJ/mol)	Energy conversion efficiency (%)
Baseline (Avg.)	149	293	19–4137	312–706 367	37–84
Annealed (Avg.)	172	339	28–413	367–752	44–90
1% SiO_2 (Avg.)	208	411	43–413	453–824	54–98
2% SiO_2 (Avg.)	203	401	41–413	442–814	52–97

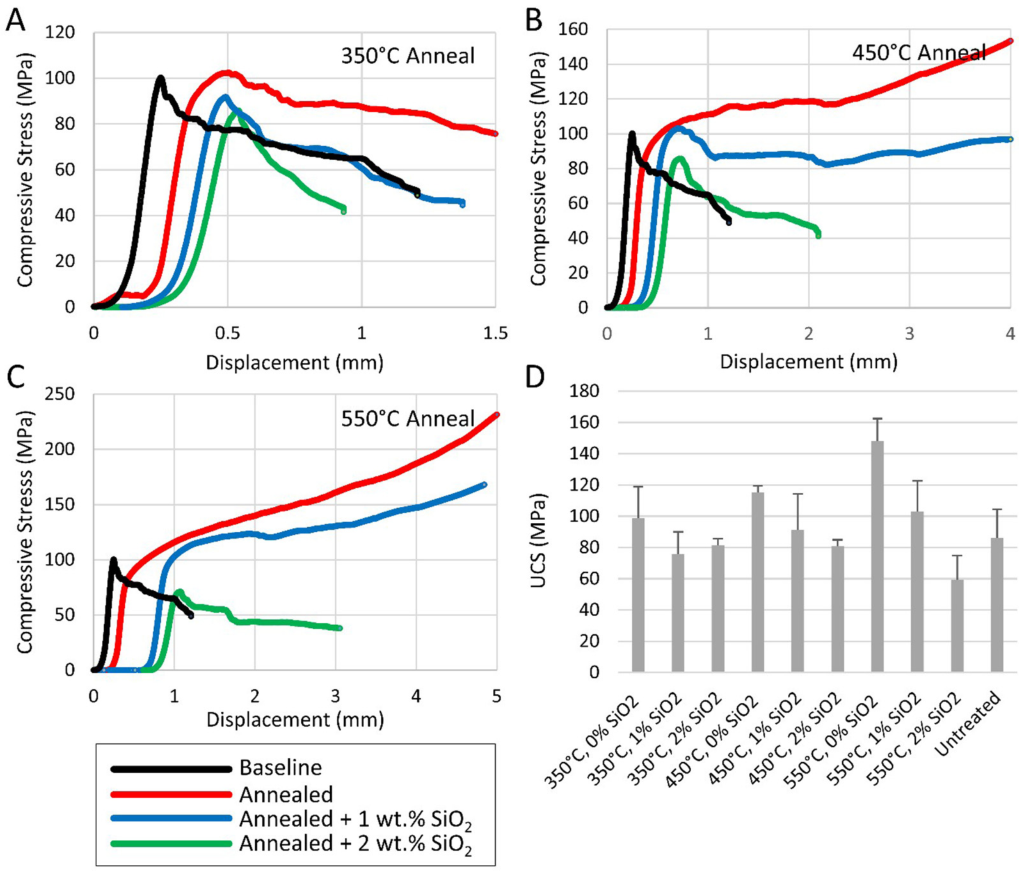

FIG. 7. Representative mechanical stress-displacement curves including baseline (black), annealed with no additive (red), 1 wt. % SiO_2-added (blue), and 2 wt. % SiO_2-added (green) for annealing temperature of (a) 350, (b) 450, (c) 550 °C as indicated on each graphic. (d) Summary of ultimate compressive stress (UCS) for all treatments. Note that for case 550 °C, 0 wt. % SiO_2, the reported value is the lower limit of failure, due to instrument capability, not the UCS since the sample does not fail under the testable conditions of the instrument.

Microscopy

Microscopy shows the physical interaction between Al and SiO_2 particles. Aluminum particles are spherically shaped and SiO_2 particles are irregularly shaped with distinctive features. No sintering between particles is observed for any samples, including those annealed to 550 °C.

SiO_2 was added to create defect sites that promote fragmentation upon impact. While the images shown in Fig. 8 were derived from compressive loading using a manual press, the fracture and debonding behavior observed provides insight into potential mechanisms resulting from discontinuous material interfaces. Starting with Fig. 8(a), three fragmented sections of a pellet are shown. A clear ridge of SiO_2 appears in the front and center image. This ridge may have been a dominant fracture point and a possible initiation site for crack formation. The conclusion is based on observation of no aluminum particles on its visible surface, and its jagged and irregular morphology. The SiO_2 site in Fig. 8(a) is an example of debonding resulting from a hard, inclusionary additive.

A fragmentation site was observed in Fig. 8(b) and an obvious fracture path is indicated with arrows. The fracture appears to begin at the SiO_2 face on top of the image (i.e., where a "V" shape is cut in SiO_2) and travels through the SiO_2 face, and down into the coalesced aluminum powder, where the fracture line closes. Interestingly, the crack completely passed through the SiO_2 on top, before closing in the Al, which illustrates the brittle fracture behavior of SiO_2 and the ductile nature of Al particles. Figure 8(b) suggests SiO_2 provides an origin for crack initiation, then promotes fragmentation or crack propagation into the Al powder. Like Fig. 8(a), notice the debonding effect of the SiO_2 face being devoid of Al particles in Fig. 8(b). Similarly, Fig. 8(c) shows multiple silica faces as the interstitial defect sites and Fig. 8(d) shows higher magnification of silica protruding from an Al particle bed with no sintering observed. Figure 8(e) chemically distinguishes the SiO_2 particles from the Al particles with spectroscopy of the surface indicated. Note the composition is indicated in the inset of Fig. 8(e), consistent with SiO_2.

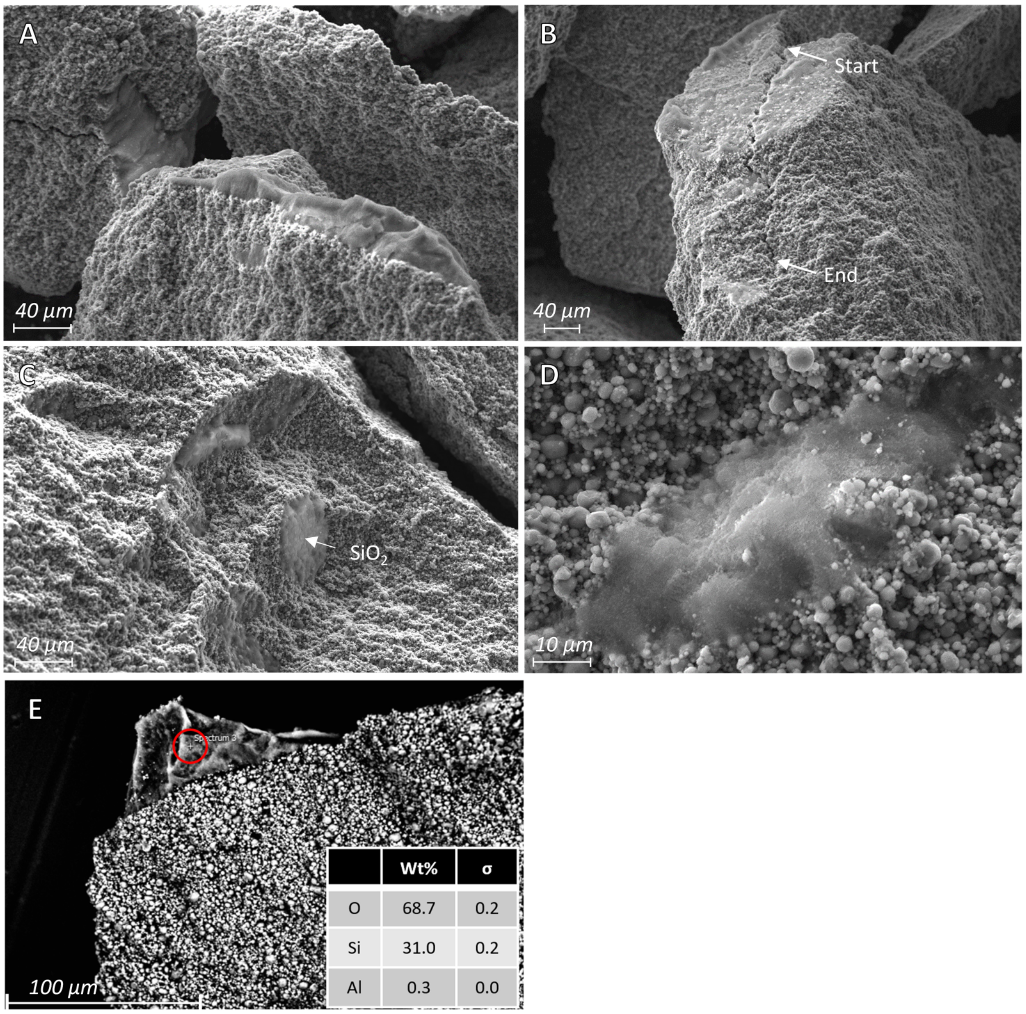

FIG. 8. (a) Image showing a SiO_2 ridge along a fragmented pellet, representing debonding between the two constituent materials (annealed 450 °C, 2 wt. % SiO_2). (b) A fracture pattern along a crushed pellet grain just before failure. Fracture starts at the SiO_2 particle and travels into the Al powder (annealed 450 °C, 2 wt. % SiO_2). (c) Display of multiple silica structures protruding from aluminum powder (annealed 550 °C, 2 wt. % SiO_2). (d) High magnification showing silica protruding from Al particle bed (annealed 550 °C, 2 wt. % SiO_2). (e) SEM image using backscattered electrons to identify SiO_2 particles in the pellet matrix. Note the SiO_2 particle with the instrument marker in red, and the inset shows the elemental components of the identified area.

DISCUSSION

Thermal energy from annealing induces a more ordered and regular arrangement of particles in the consolidated matrix, as illustrated in the cartoons of Fig. 3. Annealing progressively reduces dislocations as well as lowers surface energy in bulk and powder aluminum.[29,30,31] Figure 7 shows UCS is dramatically increased with annealing compared to the baseline, owing to the thermally activated mechanism of dislocation recovery, residual stress healing, and altered particle interface properties. Dislocation recovery induced by annealing is a key mechanism for the projectile ability to survive the launch conditions.

The introduction of SiO_2 provides irregularly hard inclusions, which manifest stress and facilitate de-bonding directly at particle interfaces [as seen in Fig. 8(a)]. Zulkoffli *et al.*[29] explain that hard inclusions in a matrix act as barriers to the movement and recovery of adjacent dislocations when moderate annealing is applied. When annealing Al composites with hard particle additives, they observed a high density of dislocations adjacent to the inclusionary particles, yet little to none in the surrounding matrix. Shang and Ritchie[32] also state that including brittle particles in an alloy can reduce ductility by an order of magnitude, and a similar trend is seen in Fig. 7(d). The results summarized in Figs. 7 and 8 are consistent with Refs. 29 and 32. At the lower annealing temperatures of 350–450 °C, the dislocations in the Al portion of the matrix are recovered and produce increased UCS to survive launch, yet the dislocations surrounding SiO_2 induce cracking and fragmentation upon impact.

There is not a direct link between UCS in Fig. 7 and combustion performance (Table III). Instead, the mechanism is implicitly realized from two stages of UCS behavior. First, the initial increased UCS upon annealing indicates strength of the pellet to survive launch. Second, the reduced UCS by inclusion of SiO_2 is evidence that crack nucleation generators incite fragmentation, which will ultimately lead to more complete combustion. While the UCS of pellets with SiO_2 inclusions is at the same general value as the untreated pellets, the annealing process glues the matrix together despite the stress concentrators and enables the projectile to survive launch but produce more complete combustion from activated fragmentation.

CONCLUDING REMARKS

Baseline, untreated aluminum projectiles show significant variability in fracture upon launch and combustion performance upon impact. Consolidating powders into pellets by cold pressing is not conducive to creating projectiles that can remain intact upon ballistic gun launch. Results revealed highly stochastic performance lacking reproducibility. This study applied a design of experiments statistical multivariant approach to examine processing conditions (i.e., factors included annealing and additives) that affect properties [ultimate compressive stress (UCS) and combustion (i.e., peak pressure)] and influence performance (i.e., energy conversion efficiency).

The UCS increased from 85 MPa for untreated (baseline) projectiles to between 100 and 150 MPa for annealing from 350–550 °C, respectively. The increased UCS is evidence of dislocation recovery and residual stress healing within the consolidated powder matrix attributed to thermal energy from annealing. Also, annealing produced projectiles that remained intact upon launch with high repeatability in combustion performance. However, annealing alone did not optimize energy conversion efficiency upon projectile impact. Vented chamber calorimetry studies show annealed projectiles fragmented upon impact to induce an increased energy conversion efficiency from 84% for untreated projectiles up to 90% for all annealing treatments.

Optimization in energy conversion efficiency was achieved by adding silica (SiO_2) inclusions to the Al powder matrix, followed by annealing. The inclusions add stress concentrators for crack nucleation and fragmentation that are activated upon ballistic impact. Microscopy of fractured projectiles showed evidence of debonding and cracking produced by silica inclusions. The annealing treatment essentially glues the projectile together and enabled it to survive launch, but the silica additive induced greater fragmentation upon impact, leading to increased energy conversion efficiency up to 98%.

Combining processing treatments to tailor an outcome requires a statistical design of experiments approach when multiple variants are considered. The approach shown in this study linked material properties to reactive properties and can be applied to other applications where controlled fragmentation is desired. Future research should be extended to investigating the theory of dislocation recovery and testing additives in various compositions or morphologies to further tailor fragmentation and combustion performance.

ACKNOWLEDGMENTS

The authors are grateful for support from the Office of Naval Research under ONR Grant Nos. N00014-19-1-2006 and N00014-21-1-2519 and our program managers, Dr. Chad Stoltz, and Dr. Michael Simpson, respectively. The Department of Energy is also gratefully acknowledged for support from Grant No. DE-NA0003988 and our program manager, Dr. Betsy Snell. Also, a special thank you to Mr. Joseph Pantoya for his assistance throughout testing, Mr. Colton Cagle for experimental support, and Ms. Samantha Knoth for instruction on the design of experiments software. The authors S.G., M.G., and T.F. acknowledge North Dakota EPSCOR for funding.

AUTHOR DECLARATIONS

Conflict of Interest

The authors have no conflicts to disclose.

Author Contributions

Alan Williams: Conceptualization (equal); Data curation (lead); Formal analysis (lead); Investigation (equal); Methodology (equal); Writing – original draft (lead). **Mackenzie Geigle:** Investigation (supporting). **Timothy Fah:** Investigation (supporting). **Surojit Gupta:** Supervision (supporting). **Michelle Pantoya:** Funding acquisition (lead); Investigation (supporting); Project administration (lead); Resources (lead); Supervision (equal); Writing – review & editing (equal).

DATA AVAILABILITY

The data that support the findings of this study are available from the corresponding author upon reasonable request.

REFERENCES

[1] S. Wang, J. Kline, B. Miles, and J. P. Hooper, "Reactive fragment materials made from an aluminum–silicon eutectic powder," J. Appl. Phys. **128**(6), 065903 (2020).

[2] H. Wang, Y. Zheng, Q. Yu, Z. Liu, and W. Yu, "Impact-induced initiation and energy release behavior of reactive materials," J. Appl. Phys. **110**(7), 074904 (2011).

[3] J. Kline and J. P. Hooper, "The effect of annealing on the impact fragmentation of a pure aluminum reactive material," J. Appl. Phys. **125**(20), 205901 (2019).

[4] B. E. Homan, K. L. McNesby, J. Ritter, J. Colburn, and A. Brant, *Characterization of the Combustion Behavior of Aluminum-Nickel Based Reactive Materials* (Defense Technical Information Center, 2009).

[5] H.-f. Wang, J.-w. Xie, C. Ge, H.-g. Guo, and Y.-f. Zheng, "Experimental investigation on enhanced damage to fuel tanks by reactive projectiles impact," Defence Technol. **17**(2), 599–608 (2021).

[6] B. R. Clark and M. L. Pantoya, "The aluminium and iodine pentoxide reaction for the destruction of spore forming bacteria," Phys. Chem. Chem. Phys. **12**(39), 12653–12657 (2010).

[7] A. P. Shaw, G. Diviacchi, E. L. Black, J. D. Moretti, R. K. Sadangi, H. A. Grau, and R. A. Gilbert, "Versatile boron carbide-based visual obscurant compositions for smoke munitions," ACS Sustain. Chem. Eng. **3**(6), 1248–1254 (2015).

[8] K. R. Bratton, K. J. Hill, C. Woodruff, L. L. Campbell, C. B. Cagle, M. L. Pantoya, J. Magallanes, J. Abraham, and C. Meakin, "High velocity impact testing of intermetallic projectiles," J. Dyn. Behav. Mater. **6**, 236–245 (2020).

[9]C. Cagle, K. J. Hill, C. Woodruff, M. L. Pantoya, J. Abraham, and C. Meakin, "Target penetration and impact analysis of intermetallic projectiles," Int. J. Impact Eng. **136**, 103427 (2020).
[10]H. Ren, W. Li, and J. Ning, "Effect of temperature on the impact ignition behavior of the aluminum/polytetrafluoroethylene reactive material under multiple pulse loading," Mater. Des. **189**, 108522 (2020).
[11]W. Mock Jr and J. T. Drotar, "Effect of aluminum particle size on the impact initiation of pressed PTFE/Al composite rods," AIP Conf. Proc. **995**(1), 971–974 (2007).
[12]H. G. Broemel, See www.quickload.co.uk for "Interior Ballistics Program for Ammunition Development and for Experienced Handloaders [QuickLOAD version 3.9]," JMS Sporting.
[13]D. A. Wiegand, B. Redingius, K. Ellis, and C. Leppard, "Pressure and friction dependent mechanical strength – cracks and plastic flow," Int. J. Solids Struct. **48**(11–12), 1617–1629 (2011).
[14]C. R. Hicks and K. V. Turner, Jr., *Fundamental Concepts in the Design of Experiments* (Oxford University Press, New York, 1999).
[15]H. Wu, J. Titchmarsh, S. Roberts, and B. Derby, "Crack healing in an alumina/silicon carbide nanocomposite after grinding and annealing," in *Symposium F—Nanophase & Nanocomposite Materials II* (MRS, 1999), Vol. 581, MRS Online Proceedings Library.
[16]M. Stumpf, T. Fey, K.-i. Kakimoto, and P. Greil, "Nb_2AlC-particle induced accelerated crack healing in ZrO_2-matrix composites," Ceram. Int. **44**(16), 19352–19361 (2018).
[17]S. K. Ghosh, *Self-healing Materials Fundamentals, Design Strategies, and Applications* (Wiley-VCH, Weinheim, 2009).
[18]O. Kolednik and K. Unterweger, "The ductility of metal matrix composites—Relation to local deformation behavior and damage evolution," Eng. Fracture Mech. **75**(12), 3663–3676 (2008).
[19]A. Bachmaier and R. Pippan, "Effect of oxide particles on the stabilization and final microstructure in aluminum," Mater. Sci. Eng. **528**(25–26), 7589–7595 (2011).
[20]F. Zhang, "Some issues for blast from a structural reactive material solid," Shock Waves **28**, 693–707 (2018).
[21]K. H. Buschow, M. Flemings, and R. Cahn, *The Encyclopedia of Materials Science and Technology* (Elsevier, Oxford, 2001).
[22]R. G. Forman, "Study of fatigue crack initiation from flaws using fracture mechanics theory," Eng. Fracture Mech. **4**(2), 333–345 (1972).
[23]Z. Chen and K. Tokaji, "Effects of particle size on fatigue crack initiation and small crack growth in SiC particulate-reinforced aluminium alloy composites," Mater. Lett. **58**(17–18), 2314–2321 (2004).
[24]W. Li, J. Chen, J. J. He, Y. J. Ren, W. Qiu, S. Q. Zhu, and Y. P. Sun, "Effect of the SiC particle orientation anisotropy on the tensile properties of a spray-formed SiC/Al-Si composite," Strength Mater. **46**(2), 221–228 (2014).
[25]M. Park, J. Yoo, and D.-T. Chung, "An optimization of a multi-layered plate under ballistic impact," Int. J. Solids Struct. **42**(1), 123–137 (2005).
[26]R. G. Ames, "Vented chamber calorimetry for impact-initiated energetic materials," in *43rd AIAA Aerospace Sciences Meeting and Exhibit, Reno, NV* (AIAA, 2005).
[27]Y. Touloukian, *Thermophysical Properties of High Temperature Solid Materials*, edited by R. a. T. D. A. F. S. C. W. A. F. B. Air Force Materials Laboratory (Macmillian, New York, 1967), vol. 57, pp. 67–82.
[28]C. Croessmann, C. Cagle, P. Dube, J. Abraham, and M. Pantoya, "Thermite and intermetallic projectiles examined experimentally in simulated high and low altitude environments," J. Appl. Phys. **131**, 175904 (2022).
[29]Z. Zulkoffli, J. Syarif, and Z. Sajuri, "Fabrication of AZ61/SIC composites by powder metallurgy process," Int. J. Mech. Mater. Eng. **4**(2), 156–159 (2009).
[30]Z. Zhang, T. Liu, A. E. Smith, N. V. Medhekar, P. N. H. Nakashima, and L. Bourgeois, "Mechanisms of void shrinkage in aluminium," J. Appl. Crystallogr. **49**(5), 1459–1470 (2016).
[31]A. Williams, I. Altman, D. Burnett, E. Gutierrez Zorrilla, A. R. Garcia, C. Cagle, C. Luke Croessmann, and M. Pantoya, "Variations in aluminum particle surface energy and reactivity induced by annealing and quenching," Appl. Surf. Sci. **579**, 152185 (2022).
[32]J. K. Shang and R. Ritchie, "On the particle-size dependence of fatigue-crack propagation thresholds in SiC-particulate-reinforced aluminum-alloy composites: Role of crack closure and crack trapping," Acta Metall. **37**(8), 2267–2278 (1989).